Fragmentation of multiply charged hydrocarbon molecules C_nH^{q+} ($n \leqslant 4$, $q \leqslant 9$) produced in high-velocity collisions: Branching ratios and kinetic energy release of the H^+ fragment

K. Béroff,[1] N. T. Van-Oanh,[2] M. Chabot,[3] T. Tuna,[3] T. Pino,[1] G. Martinet,[3] A. Le Padellec,[4] Y. Carpentier,[1,*] and L. Lavergne[5]

[1]*Institut des Sciences Moléculaires d'Orsay (ISMO), UMR CNRS 8214, Université Paris Sud 11, bât.210, F-91405 Orsay Cedex, France*

[2]*Laboratoire de Chimie Physique (LCP), UMR CNRS 8000, Université Paris Sud 11, Bât.349, F-91405 Orsay Cedex, France*

[3]*Institut de Physique Nucléaire d'Orsay (IPNO), IN2P3- CNRS, Université Paris Sud 11, F-91406 Orsay Cedex, France*

[4]*Institut de Recherche en Astrophysique et Planétologie (IRAP), UMR CNRS 5187, Université de Toulouse, 9 avenue du Colonel Roche, F-31028 Toulouse Cedex 9, France*

[5]*Laboratoire de Physique Nucléaire et de Hautes Energies (LPNHE) UPMC, UPD, CNRS-IN2P3, 4 Place Jussieu, F-75005 Paris, France*

(Received 7 July 2011; published 6 September 2011)

Fragmentation branching ratios for channels involving H^+ emission and associated kinetic energy release of the H^+ fragment [KER(H^+)] have been measured for multicharged C_nH^{q+} molecules produced in high velocity (3.6 a.u.) collisions between C_nH^+ projectiles and helium atoms. For CH^{q+} ($q \leqslant 4$) molecules, measured KER(H^+) were found well below predictions of the simple point charge Coulomb model (PCCM) for all q values. Multireference configuration interaction (MRCI) calculations for ground as well as electronic excited states were performed which allowed a perfect interpretation of the CH^{q+} experimental results for low charges ($q = 2$–3) as well as for the highest charge ($q = 4$). In this last case we could show, on the basis of ionization cross sections calculations and experimental measurements performed on the same systems at slightly higher velocity (4.5 a.u.), the prominent role played by inner-shell ionization followed by Auger relaxation and could extract the lifetime of this Auger relaxation giving rise to the best agreement between the experiment and the calculations. For dissociation of C_2H^{q+} and C_3H^{q+} with the highest charges ($q \geqslant 5$), inner-shell ionization contributed in a prominent way to the ion production. In these two cases it was shown that measured KER(H^+) were in good agreement with PCCM predictions when those were corrected for Auger relaxation with the same Auger lifetime value as in CH^{3+}.

DOI: 10.1103/PhysRevA.84.032705 PACS number(s): 34.50.Gb

I. INTRODUCTION

The study of multiply charged molecules or clusters is of fundamental interest [1]. The determination of their stability, as a function of the charge and/or size for instance, is a stringent test of cohesive forces at play in the system. More information on these forces, including their evolution with internuclear distances, may be obtained through the determination of the fragmentation branching ratios, excited states lifetime measurements, or fragmentation dynamics. Although considerable progress has been achieved in the knowledge of these species, there are still unexplained behaviors, as shown for instance in a recent work dealing with the partitioning of energy in fragmenting multicharged carbon clusters [2].

Apart from these fundamental interests, the production of multicharged molecules and clusters has been found to be a tool for accessing other experimental observables. The Coulomb explosion imaging (CEI) technique, based on the coincident recording of fragments momenta from a molecule suddenly stripped of its valence electrons, has been used to extract information on the structure of a neutral molecule multi-ionized by passing through a foil [3] or submitted to intense short (few 10 fs or less) laser pulses [4,5]. The laser technique is commonly used nowadays because it can be combined with pump-probe measurements and provide access to nuclear dynamics of all sorts (dissociation, isomerization, proton migration, etc. [6,7]).

In CEI experiments, interaction potentials between two atomic fragments of charge q_i and q_j are usually assumed to be purely Coulombic, that is, proportional to $(q_i q_j)/R$ for all internuclear distances R. A way to test this hypothesis is to measure the kinetic energy of the fragments and to compare the results to predictions of the so-called point charge Coulomb model (PCCM). This type of comparison has been performed mostly in diatomic and triatomic molecules (Mathur [1]). In O_2^{q+} ($q \leqslant 11$), Werner *et al.* [8] found a good agreement between the PCCM model and the most probable kinetic energy release (KER) of the measured distribution. In H_2O^{q+} ($q \leqslant 6$) [9] and CS_2^{q+} ($q \leqslant 10$) [10], small deviations (10%–20%) between experimental KER and PCCM were observed, the experiment being systematically lower in the first case but not in the second case. In H_2O^{q+}, as later on in CO^{2+} [11], *ab initio* calculations of electronic excited states were performed and invoked to explain deviations between measured KER and PCCM predictions. The role of the molecule charge q was put forward in other works. In dissociation of CO^{q+} ($q \leqslant 7$) [12], deviations between experiment and PCCM predictions were large for the lower q values ($q =$ 2–3), and very small for $q > 3$. This result is in qualitative agreement with potential energy curves for electronic ground and excited states of Cl_2^{q+} ($q \leqslant 10$) calculated by Wright *et al.* [13].

By contrast to works performed on diatomics and triatomics, not much has been done on larger polyatomic species. Dissociation of $C_2H_2^{q+}$ ($q \leqslant 6$) was recently studied [14] but the comparison between measured KER and PCCM

*Present address: Laboratory Astrophysics Group of the Max Planck Institute for Astronomy at the Friedrich Schiller University Jena, Institute of Solid State Physics, Helmholtzweg 3, D-07743 Jena, Germany.

predictions restricted to two-body channels C^{q+}-$C^{q'+}$ (i.e., performed on the sum of various channels). The case of $C_6H_6{}^{q+}$ ($q \geqslant 4$) was investigated [15], but also in a partial way. In the present work, diatomic, triatomic, and quadriatomic molecules have been studied and KER distributions, for all channels giving rise to a H^+ fragment, measured separately. This allowed us to investigate deviations to PCCM in situations where the size and the charge are varied.

An interesting topic, mostly investigated in photoionization, refers to inner-shell ionization and the competition between dissociation and relaxation by Auger effect [16]. In collisions using highly charged ions (HCI), impact parameters are large and this inner-shell ionization only appears at very high energy [17]. When using protons or, as in our experiment, helium projectiles, inner-shell ionization is contributing at much lower energy. In the present experiments, performed at velocities of a few atomic units, prominent contribution of inner-shell ionization was found for higher charges of C_nH^{q+} molecules. The competition between dissociation and Auger relaxation, and its role in the measured KER's, has been studied in these cases as will be shown below.

As mentioned before, deviations between measurements and PCCM predictions in diatomics have often been reported and interpreted, in some cases, on the basis of population of excited states having a nonpurely Coulombic character. We did *ab initio* calculations of electronic excited states of CH^{q+} molecules (q = 1–4) within the MRCI/CASSCF approach (see Sec. VI). Whereas previous data existed (for instance Bannister *et al.* [18] for CH^+, Gu *et al.* [19] for CH^{2+}, and Butler *et al.* [20] for CH^{3+}), the specificity of our work is to have performed all calculations, including the CH^{4+} case, at the same level of accuracy and to have calculated also some states of CH^{3+} with both inner-shell and valence shell holes. Moreover, predictions of populations of these states by collision were performed, allowing a full comparison between measured and calculated KER to be conducted.

The plan of the paper is the following.

In Sec. II we present our setup and experimental methods. This study was made possible thanks to the use of the high velocity inverse kinematics mode (the molecule of interest is a high velocity projectile), ensuring 4π detection and 100% efficiency for any number of coincident fragments. We used original fragments detectors for mass and charge identification [21], operating in coincidence with a position sensitive detector (PSD) for the H^+ fragment imaging.

In Sec. III results concerning ionization cross sections of C_nH^+ projectiles colliding with helium atoms are presented. We showed here, and quantified, the role played by inner-shell ionization on the production of highly charged species as well as the role of the molecule alignment.

In Sec. IV we present measured fragmentation Branching ratios of C_nH^{q+} molecules and in Sec. V measured kinetic energy releases of the H^+ fragment [KER(H^+)] for all channels involving emission of a proton.

Discussion of experimental results, in particular with respect to PCCM predictions for KER(H^+) values, are presented in Sec. VI for CH^{q+} and in Sec. VII for C_2H^{q+} and C_3H^{q+}. In the case of CH^{q+} (q = 1–4), *ab initio* multireference configuration interaction (MRCI) calculations of electronic excited states are presented and used, together with predictions of their populations, to interpret the experimental results. Conclusions are presented in Sec. VIII.

II. EXPERIMENTAL SETUP AND METHODS

Experiments have been performed at the Tandem accelerator in Orsay, with two slightly different setups. The first setup has been described in detail recently [22] and was used for the study of ionization and fragmentation of C_nH^+ projectiles (n = 1–4) of $v_p = 4.5$ a.u. velocity colliding with a helium atom. Briefly, collisions between C_nH^+ projectiles and helium atoms occurred in a gaseous jet of known thickness [23] under single collision conditions. Fragments produced in the collision were deflected, according to their charge over mass ratios, by an intense electric field and impinged on solid-state surface barrier detectors of 100% efficiency operating in coincidence. The shape analysis of the transient current delivered by each detector allowed the mass and charge identification of all fragments impinging on it [21]. The second setup, devoted to KER(H^+) measurements, was similar to the previous one with only two modifications, namely, the use of a position sensitive detector (PSD) for the H^+ fragment and the detection of recoil He^+ and He^{++} ions in coincidence with all fragments (see Fig. 1). This setup was used for measurements of KER(H^+) distributions following excitation, ionization, and

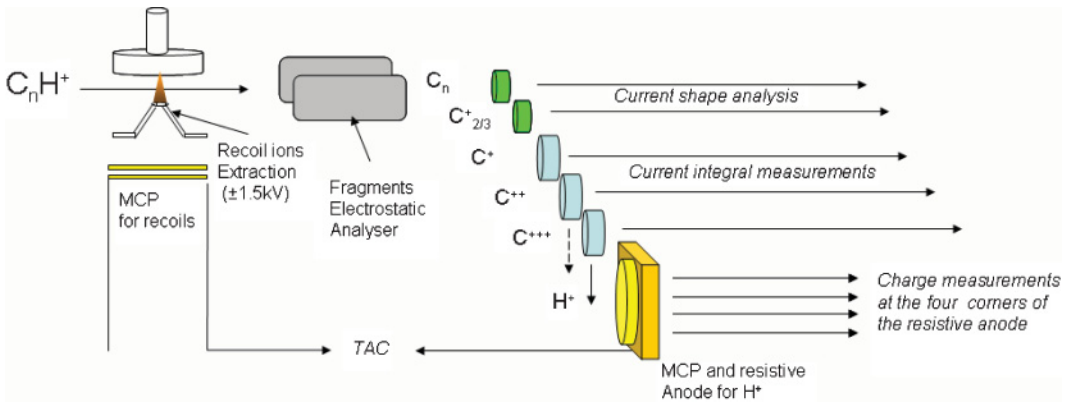

FIG. 1. (Color online) Schematic view of the experimental setup.

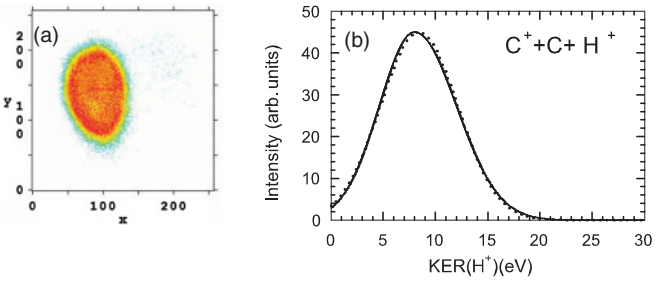

FIG. 2. (Color online) (a) H^+ image recorded onto the PSD detector following $C_2H^{2+} \rightarrow C^+|C|H^+$ dissociation; X and Y axis are, respectively, in the horizontal and vertical plane; dimensions along X and Y are in channels (1 channel = 0.167 mm). (b) KER(H^+) distribution extracted from the fit of (a) using a single Gaussian distribution (dotted line) or two half Gaussians of different widths (solid line), see text.

fragmentation of CH^+, C_2H^+, and C_3H^+ in $v_p = 3.6$ a.u. velocity collisions with a helium atom.

The PSD detector, of 40 mm diameter, was made of a three-stage microchannel plate (MCP) associated with a resistive anode for position encoding [24]. The position resolution was 0.4 mm which corresponded, in our geometrical arrangement, to an energy resolution of the order of 1 eV for KER(H^+) $\sim$ 5 eV and 2.5 eV for KER(H^+) $\sim$ 30 eV. Time arrival of the H^+ fragment was recorded using a start signal provided by a two-stage MCP placed below the gaseous jet (see Fig. 1). The time resolution ($\leqslant$1 ns) was not sufficient to extract information related to the H^+ *momentum*. Accordingly, KER(H^+) were extracted from position measurements only assuming an isotropic emission of the proton. In fact, some anisotropy in the emission of H^+ from C_nH^{q+} species n = 2–3, $q \geqslant 4$ occurred since these species are preferentially produced when the molecule is aligned with the beam. Based on angular differential ionization cross sections calculations (see Sec. III), the anisotropy was extracted and its effect on the KER(H^+) extraction quantified through a Monte Carlo simulation. We predicted that KER(H^+) values had to be increased with respect to extracted values under the isotropic assumption by 4% to 12% for C_2H^{q+} (q = 4–7) and 6% to 24% for C_3H^{q+} (q = 4–6). The coincident detection of He^{q+}

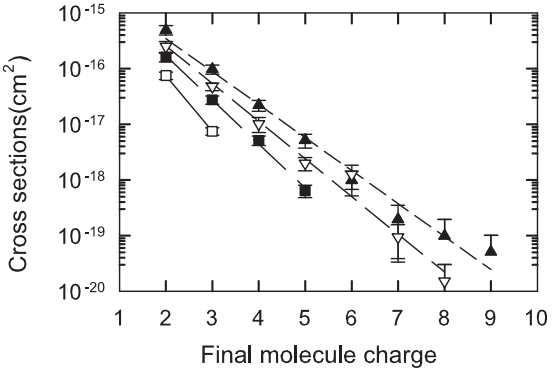

FIG. 3. Measured ionization cross sections of CH^+ (open squares), C_2H^+ (full squares), C_3H^+ (open triangles), and C_4H^+ (full triangles) in collisions with He at $v_p = 4.5$ a.u.; lines are to guide the eye.

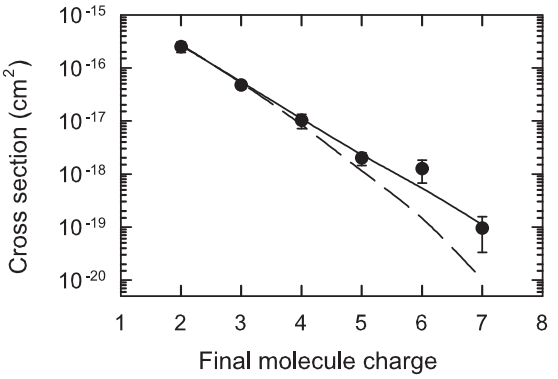

FIG. 4. Comparison between measured and calculated ionization cross sections in $v_p = 4.5$ a.u. C_3H^+-He collisions. Black dots: experimental results; solid line: results of the IAE model (see text); dashed line: results of the IAE model without autoionization.

recoils was nevertheless useful since it allowed selection of events occurring in the jet only with an excellent signal to background ratio ($\sim$2000). The jet was operating at relatively high pressure ($n_{\text{jet}}\Delta x \sim 2 \times 10^{14}$ atoms/cm^2) and some double collisions, contributing to 10% of the ion production, had to be subtracted.

In Fig. 2(a) is shown an H^+ fragment image, obtained in dissociation of C_2H^{2+} into $C^+|C|H^+$. The special shape of the image, nonsymmetrical and slightly distorted, originates from two effects: a shrinking along the X axis due to the electric field of the fragments electrostatic analyzer (i) and a deformation, mostly along Y, induced by the electric field placed at the jet location for acceleration of helium recoil ions (ii). Both effects were simulated in the particular arrangement of the experiment using the SIMION code (SIMION 3D version 6.0) for different H^+ energies, beam positions, and electric field values. In Fig. 2(b) we show the KER(H^+) distribution extracted from treatment of Fig. 2(a). Two distributions are actually presented, one (the dotted line) obtained by assuming a Gaussian shape for the KER(H^+) distribution, the other one (solid line) obtained with an asymmetrical kinetic energy distribution made of two half Gaussians of different standard deviations placed at the same position. The two fits give almost identical results. The two types of shapes were systematically tried for all channels. Results are presented below. They show that close KER(H^+) distributions were obtained with the two shapes, most probable values (mean values) differing by 3% (1%) when an averaging over all channels is performed. Error bars on experimental KER(H^+) values were 10% and 20% on the low and high energy side, respectively, originating from statistics, double collisions subtraction, and ion optics correction.

III. IONIZATION CROSS SECTIONS IN C_nH^+ -He COLLISIONS

Ionization cross sections in collisions of $v_p = 4.5$ a.u. C_nH^+ projectiles with He atoms are presented in Fig. 3. As seen in this figure, cross sections for production of highly charged molecules are rather large. For high enough charges, inner shell ionization (1s shell of carbon atoms) followed by autoionization plays a large role. For showing that, we made calculations of ionization cross sections using the

TABLE I. Percentages (%) of C_nH^{q+} ion production involving single (and double in parentheses) inner-shell ionization followed by Auger relaxation, as calculated with the IAE model (see text). Missing percentages, with respect to total of 100%, are due to pure valence ionization.

q	3	4	5	6	7
CH^{q+}	26	76			
C_2H^{q+}	11	38	60 (10)	53 (39)	29 (67)
C_3H^{q+}	9	27	48 (5)	57 (19)	

independent atom and electron (IAE) collision model [25] including both valence and inner-shells ionization [22]. The CH^+ internuclear distance was taken equal to 1.13 Å [26], whereas for C_2H^+ and C_3H^+, assumed to be linear with the H atom at the end of the chain [27,28], interatomic distances equal to 1.3 Å (r_{C-C}) and 1.1 Å (r_{C-H}) in C_2H^+ and 1.34 Å ($r_{C-C'}$), 1.23 Å ($r_{C'-C''}$) and 1.08 Å ($r_{C''-H}$) in C_3H^+ were considered. As seen in Fig. 4 for the case of C_3H^+ projectiles, inner-shell ionization followed by autoionization must be introduced in order to reproduce experimental cross sections. These calculations predicted that the smaller the molecule, the larger the role played, at fixed final charge, by inner-shell ionization.

Calculations using the IAE model were also performed for the case of incident C_nH^+ projectiles of 3.6 a.u. velocity using impact parameter probabilities calculated at this velocity. The role of inner-shell ionization was also found important, as shown in Table I. In this Table, the contribution of inner-shell ionization to the ion production is reported, the missing percentage corresponding to pure valence ionization

TABLE II. Experimental results concerning dissociation BR and KER(H^+) distributions. Columns 4 and 5: partial BR of C_nH^{q+} molecules (at fixed n, q values) for channels involving H^+ emission in collisions at $v_p = 3.6$ a.u. (column 4) and $v_p = 4.5$ a.u. (column 5); error bars for BR of column 5 can be found in the Appendix. Characteristics of measured KER(H^+) distributions (columns 6 to 9) measured in $v_p = 3.6$ a.u. collisions obtained: by assuming a Gaussian shape distribution: $\exp -[(E - E_1)^2/2{\sigma_1}^2]$ (columns 6 and 7) or an asymmetric distribution made of two half Gaussian distributions centered in E_2 and having standard deviations σ_{2L} (low energy side) and σ_{2H} (high energy side) (columns 8 and 9). Energies are having (+20%, −10%) relative error bars (see Experimental section).

System	q	Channel	BR (3.6 a.u.)	BR (4.5 a.u.)	E_1 (eV)	σ_1 (eV)	E_2 (eV)	σ_{2L}; σ_{2H} (eV)
CH^{q+}	1	$C\|H^+$			4.0	3.0	3.5	2.3; 3.4
	2	$C^+\|H^+$			7.9	2.7	7.2	2.1; 3.2
	3	$C^{++}\|H^+$			16.4	6.5	17.9	7.7; 5.2
	4	$C^{3+}\|H^+$			20.7	8.4	23.5	10.5; 5.9
C_2H^{q+}	1	$C_2\|H^+$	0.20	0.15	0.9	2.8	0.1	0.1; 3.2
		$C\|C\|H^+$	1	1	1.2	3.1	0.3	0.2; 3.5
	2	${C_2}^+\|H^+$	0.93	1	6.0	2.0	5.6	1.8; 2.3
		$C^+\|C\|H^+$	1	1	8.4	3.7	8.0	3.4; 4.0
	3	$C^+\|C^+\|H^+$	1	1	15.1	4.7	16.2	5.6; 3.7
		$C^{2+}\|C\|H^+$	0.11	0.08	15.1	6.6	17.7	8.8; 4.3
	4	$C^{2+}\|C^+\|H^+$	1	1	22.2	7.6	25.3	10.0; 5.2
		$C^{3+}\|C\|H^+$	0.01	$< 5 \times 10^{-3}$	11.8	13.3	12.8	15.9;12.8
	5	$C^{2+}\|C^{2+}\|H^+$	1	–	30.0	9.3	33.3	11.9; 6.8
		$C^{3+}\|C^+\|H^+$	0.35	–	26.5	10.2	30.4	13.1; 7.1
	6	$C^{3+}\|C^{2+}\|H^+$			35.6	10.9	39.2	13.4; 7.9
	7	$C^{3+}\|C^{3+}\|H^+$			41.5	7.1	43.8	8.8; 5.3
C_3H^{q+}	1	$C_3\|H^+$			1.5	1.4	0.8	0.4; 1.8
		$C_2\|C\|H^+$			1.3	2.1	0.1	0.05; 2.7
		$C\|C\|C\|H^+$			6.5	6.6	6.5	7.9; 6.6
	2	${C_3}^+\|H^+$	–	1	8.5	4.2	8.3	4.1; 4.3
		${C_2}^+\|C\|H^+$	0.15	0.19	6.1	2.7	5.6	2.3; 3.1
		$C^+\|C_2\|H^+$	0.11	0.16	5.3	2.5	4.7	2.0; 3.0
		$C^+\|C\|C\|H^+$	0.32	0.32	7.3	3.3	6.5	2.7; 4.0
	3	${C_2}^+\|C^+\|H^+$	0.55	0.50	10.7	3.5	10.8	3.6; 3.5
		$C^+\|C^+\|C\|H^+$	1	1	12.7	3.8	12.6	4.2; 4.3
		$C_2\|C^{2+}\|H^+$	3.4×10^{-3}	2×10^{-3}	9.7	6.2		
		$C^{2+}\|C\|C\|H^+$	0.024	0.020	12.9	4.2	10.4	1.9; 6.1
	4	$C^+\|C^+\|C^+\|H^+$	1	1	19.5	6.6	22.0	8.5; 4.5
		${C_2}^+\|C^{++}\|H^+$	0.020	0.014	13.9	8.1	18.5	11.6; 4.1
		$C\|C^+\|C^{++}\|H^+$	0.26	0.26	18.3	8.5	17.8	8.0; 8.9
	5	$C^+\|C^+\|C^{++}\|H^+$	1	1	27.4	9.1	28.4	9.8; 8.4
		$C\|C^{2+}\|C^{2+}\|H^+$	0.04	0.04	32.8	4.4	25.5	2.4; 9.0
	6	$C^+\|C^{2+}\|C^{2+}\|H^+$	1	1	36.4	9.5	36.6	9.6; 9.5
		$C^+\|C^+\|C^{3+}\|H^+$	0.18	0.12	32.4	11	32.9	11.5;10.7

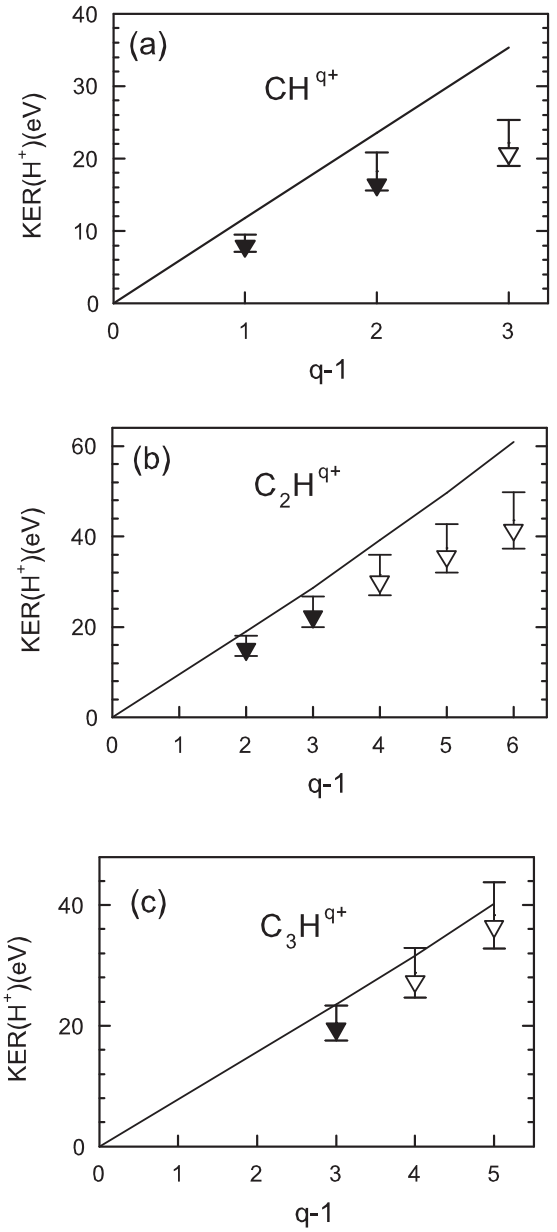

FIG. 5. Comparison between measured and calculated KER(H^+) in dissociation of C_nH^{q+}. (a) Dissociation of CH^{q+} into $C^{(q-1)+}$-H^+ channels. (b) Dissociation of C_2H^{q+} into $C^+|C^+|H^+$, $C^{2+}|C^+|H^+$, $C^{2+}|C^{2+}|H^+$, $C^{3+}|C^{2+}|H^+$, and $C^{3+}|C^{3+}|H^+$ channels for $q = 3$, 4, 5, 6, and 7, respectively. (c) Dissociation of C_3H^{q+} into $C^+|C^+|C^+|H^+$, $C^{2+}|C^+|C^+|H^+$, and $C^{2+}|C^{2+}|C^+|H^+$ channels for $q = 4$, 5, and 6, respectively. Open triangles refer to cases where inner-shell ionization contributes in a prominent way (>50%) to the ion production. Solid lines refer to predictions of the PCCM model.

(for instance, CH^{4+} being produced at 76% by inner-shell ionization followed by autoionization-plus valence ionization versus 24% for triple valence ionization).

We also looked at the angular dependence of ionization cross sections. Indeed, using the IAE model, it was predicted long ago that large ionization degrees of a molecule are better reached when the molecule is aligned along the beam [25], a theoretical prediction checked experimentally [29]. We performed calculations of differential C_nH^+ ionization cross

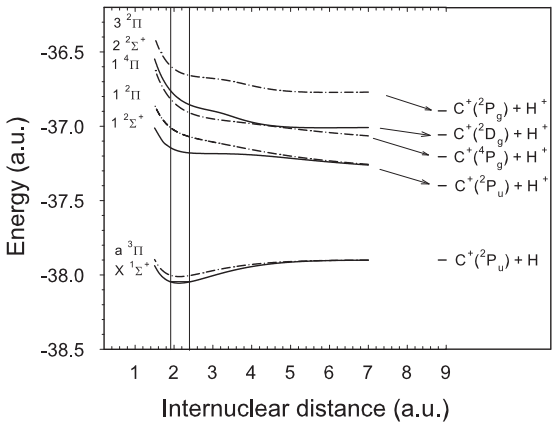

FIG. 6. MRCI potential energy curves of states of CH^+ (the two lowest curves) and CH^{2+} (the five highest curves), together with dissociation limits, relevant to interpretation of measured KER after dissociation of CH^{2+}. The two vertical lines refer to the Franck-Condon region from $v = 0$.

sections $d\sigma/d\Theta$ (Θ being the molecule-beam axis angle) and compared the results to the isotropic sin Θ law. No alignment was predicted for CH^{q+} production cross sections. As to C_nH^{q+} $n = 2$–3 $q \geqslant 4$ production cross sections, a slight distortion of the isotropic function in favor of lower Θ values was obtained, with a reduction of the mean value by 4%, 7%, 11%, and 8% for C_2H^{q+} $q = 4$, 5, 6, and 7 and by 7%, 14%, and 20% for C_3H^{q+} $q = 4$, 5, and 6, respectively as compared to the isotropic case (57.29°). We remark from these values that the alignment is predicted larger, at fixed final charge, when the molecule is longer. Based on these calculations, we derived corrected factors on experimentally extracted KER(H^+) values, as discussed in the Experimental section.

IV. BRANCHING RATIOS OF DISSOCIATION OF MULTIPLY CHARGED MOLECULES

A. Data for incident C_nH^+ ($n \leqslant 4$) projectiles at 4.5 a.u.

Using the first setup, all branching ratios for dissociation of C_nH^{q+} species ($n \leqslant 4$, $q \leqslant 9$) could be extracted. Branching ratios (BR) for most prominent channels of dissociation are

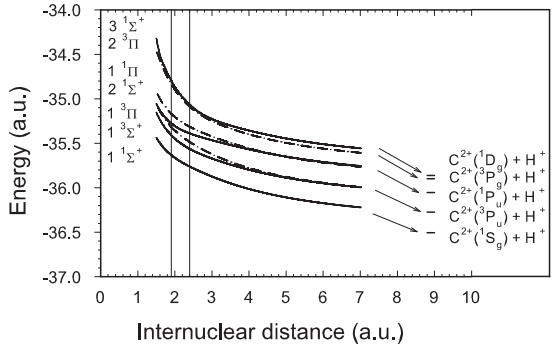

FIG. 7. MRCI potential energy curves of states of CH^{3+}, together with dissociation limits, relevant to the interpretation of KER measurements following dissociation of CH^{3+}. The two vertical lines refer to the Franck-Condon region.

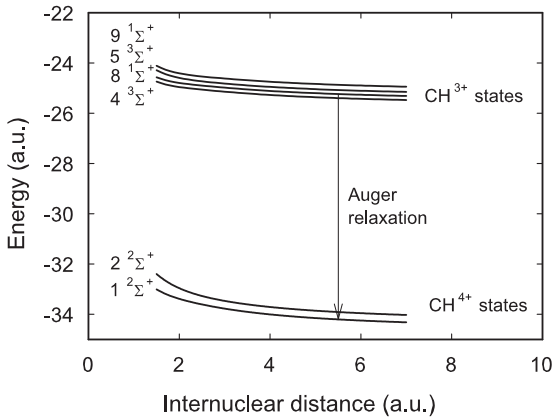

FIG. 8. MRCI calculations of potential energy curves of CH^{3+} states with one inner-shell vacancy (the four top states) together with MRCI calculations of CH^{4+} states with all ionization in the valence shells (the two bottom states) pertinent to interpretation of measured KER following dissociation of CH^{4+}.

given in the Appendix. More precisely, only channels having BR $\geqslant 1\%$ and channels whose KER(H^+) have been measured have been reported; the reader interested in the complete set of data may find it elsewhere [30].

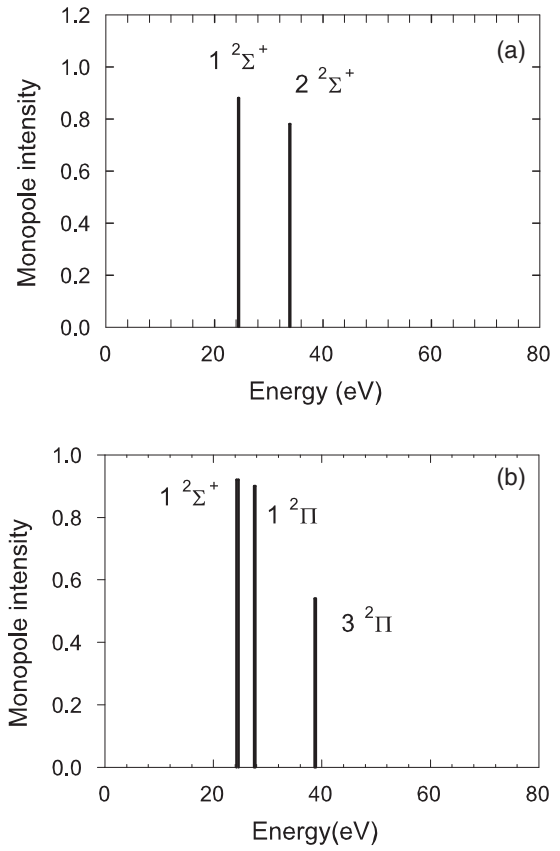

FIG. 9. Monopole intensities for various final states of CH^{2+}, starting from the ground state $X^1\Sigma^+$ (a) or from the metastable $a^3\Pi$ (b) of CH^+. Energies are referenced with respect to the ground state of CH^+.

TABLE III. Population of final states of CH^{2+} by valence single ionization of CH^+. Predictions are based on the use of Eq. (1) and development of initial and final wave functions in main configurations (see text). The initial wave function is the ground state of CH^+ except for values in parentheses where it is the metastable state $a^3\Pi$ state of CH^+.

State of CH^{2+}	Intensity
$1^2\Sigma^+$	0.88 (0.92)
$2^2\Sigma^+$	0.78
$3^2\Sigma^+$	0
$1^2\Pi$	(0.90)
$2^2\Pi$	(0)
$3^2\Pi$	(0.54)

B. Data for incident C_nH^+ ($n \leqslant 3$) projectiles at 3.6 a.u.

Only channels with H^+ emission were recorded in this experiment, performed with the second setup. In Table II, column 4, are shown measured partial dissociation BR of C_nH^{q+} (within fixed n, q values) at $v_p = 3.6$ a.u. In order to make a comparison, we reported in column 5 values measured at $v_p = 4.5$ a.u. Very similar results are obtained with the two projectile velocities, which makes sense.

V. RESULTS ON KER(H^+) DISTRIBUTIONS IN C_nH^{q+} ($n \leqslant 3$, $q \leqslant 7$) DISSOCIATIONS

In Table II, columns 6–9, are presented characteristics of KER(H^+) distributions measured in 3.6 a.u. C_nH^+-He collisions by assuming a Gaussian shape distribution $\exp -[(E - E_1)^2/2{\sigma_1}^2]$ (columns 6 and 7) or an asymmetric distribution made of two half Gaussian distributions centered in E_2 and having standard deviations σ_{2L} (low energy side) and σ_{2H} (high energy side) (columns 8 and 9). Most probable values are then E_1 or E_2 according to the shape of the distribution used. As mentioned before, small differences between these two values are observed. All experimental energies are having (+20%, −10%) relative error bars (see Experimental section).

As discussed in the Introduction, it is interesting to compare the measured KER(H^+) values with predictions of the simple point charge Coulomb model (PCCM). In this model, point

TABLE IV. Population of final states of CH^{3+} by valence double ionization of CH^+. Predictions are based on the use of Eq. (2) and development of initial and final wave functions in main configurations (see text). The initial wave function is the ground state of CH^+ except for values in parentheses where it is the metastable state $a^3\Pi$ state of CH^+.

State of CH^{3+}	Intensity
$1^1\Sigma^+$	0.87 (0.88)
$2^1\Sigma^+$	0.81 (0.83)
$3^1\Sigma^+$	0.69 (0)
$1^3\Sigma^+$	0.92 (0.94)
$1^1\Pi$	(0.88)
$1^3\Pi$	(0.94)
$2^3\Pi$	(0.96)

TABLE V. Same legend as Table IV but for states populated by single valence plus single inner-shell ionization of CH^+.

State of CH^{3+}	Intensity
$8^1\Sigma^+$	0.75
$9^1\Sigma^+$	0.65
$4^3\Sigma^+$	0.81
$5^3\Sigma^+$	0.73

charges (ionic charges) are positioned at the atomic sites of the molecule which then relaxes under action of pure Coulomb repulsive forces. We made this comparison in Fig. 5 for CH^{q+} [$C^{(q-1)+}$-H^+ channels, Fig. 5(a)], C_2H^{q+} [$C^+|C^+|H^+$, $C^{2+}|C^+|H^+$, $C^{2+}|C^{2+}|H^+$, $C^{3+}|C^{2+}|H^+$, and $C^{3+}|C^{3+}|H^+$ channels for $q = 3$, 4, 5, 6, and 7, respectively, Fig. 5(b)], and C_3H^{q+} [$C^+|C^+|C^+|H^+$, $C^{2+}|C^+|C^+|H^+$, and $C^{2+}|C^{2+}|C^+|H^+$ for $q = 4$, 5, and 6, respectively, Fig. 5(c)]. Experimental results (E_1 values of Table II) are shown by triangles where full triangles refer to cases dominated ($\geqslant$50%) by pure valence ionization and open triangles refer to cases where inner-shell ionization dominates the ion production. Predictions of PCCM are shown by solid lines. They were obtained, exception made of the trivial CH^{q+} case, by running a FORTRAN code of classical molecular dynamics generated by Coulomb repulsive forces. For "nonsymmetrical" channels $C^{q1+}|C^{q2+}|H^+$ with $q1 \neq q2$, we averaged PCCM predictions obtained by interchanging the two carbon atoms since the different configurations (the higher charged atom being close or far from H^+) lead to quite different KER(H^+) results (for instance 24.7 eV for $C^{2+}|C^+|H^+$ and 32.6 eV for $C^+|C^{2+}|H^+$). As seen in Fig. 5, there are large deviations between measurements and PCCM predictions that will now be discussed.

VI. INTERPRETATION OF KER RESULTS IN DISSOCIATION OF CH^{q+} MOLECULES

As shown in Fig. 5(a), large deviations between measurements and PCCM predictions are observed. As discussed in Sec. I, such a result has often been reported in diatomics and sometimes interpreted on the basis of population of excited states having a nonpurely Coulombic character [1]. We followed this approach and did calculations of electronic excited states of CH^{q+} molecules ($q = 1$–4) together with predictions of their populations (Secs. VI A and VI B, respectively). This allowed for a full comparison between measured and calculated KER to be performed (Sec. VI C).

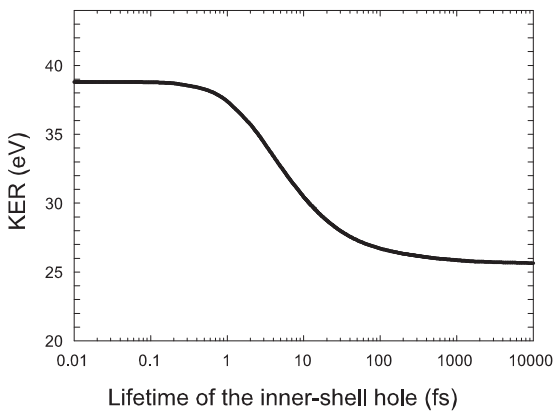

FIG. 10. Competition between dissociation and Auger relaxation: calculated variation of the KER value in dissociation of CH^{3+}, as a function of the Auger lifetime of the inner-shell hole.

A. Calculations of ground state and electronic excited states of CH^{q+} molecules

Ab initio calculations of electronic ground and excited states of CH^{q+} molecules have been performed at multireference configuration interaction-configuration active space self-consistent field level (MRCI-CASSCF) with cc-pVQZ basis set using the MOLPRO package version 2010.1 (MOLPRO [31]). In the ground and low-lying excited state calculations, full valence and core orbitals (four σ and two π orbitals) were chosen as the active space for the CASSCF calculations. For higher excited states, two σ and two π orbitals were further added in the active space while consistency of the results was checked. The number and the type of electronic states to be calculated was dictated by predictions of their populations in the collision, from the ground state ($X^1\Sigma^+$) but also from the first excited ($a^3\Pi$) state of CH^+, as explained in Sec. VI B. The population of the metastable $a^3\Pi$ state in our experiment, close in energy to the ground state ($\sim$1 eV), is probable as in all experiments using ion beams [18] although the exact amount of its contribution is unknown. Potential energy curves for all electronic states were calculated for internuclear distances between 1.5 and 7 a.u., that is, around the equilibrium distance in CH^+ (2.14 a.u., in accordance with Amitay *et al.* [26]).

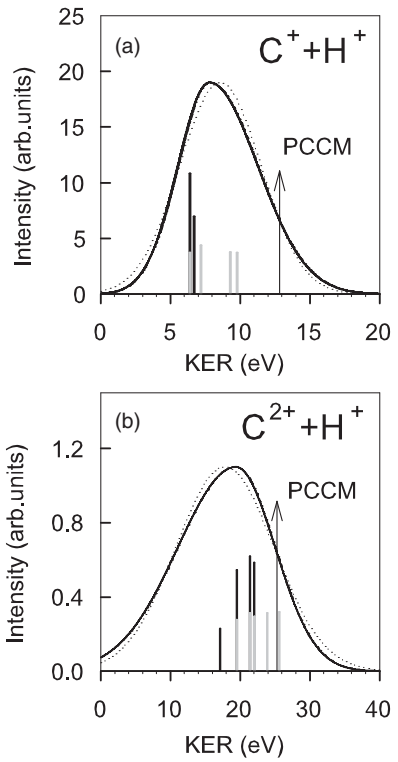

FIG. 11. Comparison between measured KER distributions (solid and dotted curves, see Sec. II) in C^+-H^+ dissociation (a) and C^{2+}-H^+ dissociation (b) and calculated KER starting from the ground state of CH^+ (vertical black lines) or from the metastable $a^3\Pi$ state of CH^+ (vertical gray lines). Arrows correspond to PCCM predictions.

TABLE VI. PCCM predictions for KER(H^+) values (in eV) for some C_2H^{q+} channels when single (S), respectively, double (D) Auger relaxation takes place on one, respectively, two carbon atoms with a lifetime equal to 0.01 fs (column 3), 10 fs (column 4), 20 fs (column 5), and 200 fs (column 6).

Final Channel		KER(H^+) (0.01 fs)	KER(H^+) (10 fs)	KER(H^+) (20 fs)	KER(H^+) (200 fs)
$C^{2+}\|C^{2+}\|H^+$	S	39.2	33.0	31.5	29.2
$C^{3+}\|C^{2+}\|H^+$	S	49.6	42.8	41.4	39.2
$C^{3+}\|C^{2+}\|H^+$	D	49.6	35.8	33.1	29.3
$C^{3+}\|C^{3+}\|H^+$	D	60.9	45.8	43.2	39.8

In Fig. 6 are reported calculated potential energy curves for CH^+ and CH^{2+} molecules. As in all figures [Figs. 6–8] the states are, exception made of the two states of CH^+, numbered within a given molecular electronic term in order of increasing energy (in the Franck-Condon region). Note that the numbering is operative even for states not represented. Four doublet states and one quartet state of CH^{2+} have been considered, predominantly populated in the collision by valence single ionization of CH^+ as explained in Sec. VI B. The lowest dissociation limit $C^+(^2P_u) + H^+$ has been calculated at the same level of accuracy than the electronic excited states (MRCI method), whereas higher energy dissociation limits were derived from the knowledge of the C^+ electronic excited state energies [32]. The kinetic energy release after ionization is obtained by the difference between the energy of the considered electronic state of CH^{2+} at 2.14 a.u. and the energy of its dissociation limit. A width of typically 2 to 3 eV for the calculated KER is associated to the Franck-Condon region, indicated by two vertical solid lines in Fig. 6. Note that a slight fraction of the incident CH^+ molecules may be in an excited vibrational state ($v = 1$ mostly) since the incident temperature, of the order of 3500 K [22], corresponds to an internal energy of 0.3 eV/degree of freedom, that is, slightly larger than the zero-point energy (0.175 eV).

In Fig. 7 we report similar curves for CH^{3+} states predominantly populated by double valence ionization of CH^+. These curves will be used for interpretation of the measured KER following dissociation of CH^{3+} molecules. The widths associated to the Franck-Condon region are here between 4 and 8 eV depending on the state.

Figure 8 was used to interpret measured KER after dissociation of CH^{4+}. The dominant process for production of CH^{4+} species from CH^+ is indeed inner-shell plus valence ionization followed by Auger effect (76%, see Table I, as compared to 24% due to triple valence ionization). In Fig. 8 the four top curves correspond to CH^{3+} states having one inner-shell hole, whereas the three lowest curves refer to CH^{4+} with all vacancies in the valence shell.

B. Predictions of populated states

Predictions of populated states have been done on the basis of two main approximations:

(1) We assumed that the electronic ground and excited states of CH^{q+} molecules are produced by pure ionization, that is, without associated electronic excitation *due to the projectile*. This statement is based on calculations of {ionization + excitation} cross sections performed within the IAE model in the C^+ ($v = 2.6$ a.u.)-helium collision. We indeed found this double process to be of the order of 10% of the exclusive ionization for the case of single ionization, and of lower magnitude for the case of double and triple ionization.

(2) We assumed that ionization cross sections are identical for all *valence* electrons.

Then the probability of reaching in the collision, by valence single ionization of an initial N-electron state Φ_0, a given final $(N-1)$ electron state Φ_f is equal to I, the intensity of the ionization peak in the monopole approximation [33]:

$$I = \sum_i |\langle \Phi_f(N-1)|a_i|\Phi_0(N)\rangle|^2, \tag{1}$$

where N is the number of electrons in the initial state and a_i the annihilation operator for molecular orbital i.

The term in brackets on the right-hand side of Eq. (1) represents the probability amplitude of being in a final state Φ_f after removing an electron in the molecular orbital i of initial state Φ_0. It has been extensively used in photoionization and photoemission studies, following the pioneer theoretical work of Martin and Shirley based on configuration interaction methods [34], referred to as the spectroscopic factor [35,36] or, for its squared value, as to the pole strength in Green's function methods [36,37]. In particular, the good account of this term for reproducing experimental photoelectron spectrum using a state-independent photoionization cross section has been demonstrated by Krummacher *et al.* [36].

We obtained monopole intensities for various final states of CH^{2+} using Eq. (1) and correlated initial and final states. For this calculation main terms, associated to coefficients greater than ± 0.3 in the development of Φ_0 and Φ_f on molecular configurations, were considered. We checked this approximation for some cases and found good agreement. In Fig. 9 and Table III are presented these monopole intensities for various final states, starting from the initial ground state of CH^+ [Fig. 9(a)] or from the metastable $a^3\Pi$ state of CH^+ [Fig. 9(b)]. Interestingly enough, the $2\,^2\Pi$ state is not predicted to be populated from the metastable state, whereas the $3\,^2\Pi$ state is populated [Fig. 9(b)]. This is due to the fact that transition from $a^3\Pi$ to $2\,^2\Pi$ would involve a 2σ ionization accompanied by a forbidden spin flip of either a 3σ or 1π electron.

Predictions of final state intensities of CH^{3+}, following double valence ionization of CH^+, were performed using a generalization of Eq. (1), namely [38],

$$I = \sum_i \sum_{j<i} |\langle \Phi_f(N-2)|a_i a_j|\Phi_0(N)\rangle|^2 \tag{2}$$

an expression involving two annihilation operators a_i and a_j.

TABLE VII. Same legend as Table VI for some C_3H^{q+} channels.

Final Channel		KER(H^+) (0.01 fs)	KER(H^+) (10 fs)	KER(H^+) (20 fs)	KER(H^+) (200 fs)
$C^+\|C^+\|C^{2+}\|H^+$	S	31.6	28.1	27.1	25.2
$C^+\|C^{2+}\|C^{2+}\|H^+$	S	40.2	35.2	33.8	31.8

As in the preceding case, terms associated to main molecular configurations of Φ_0 and Φ_f (i.e., coefficients greater than ± 0.3) were considered. Results for calculated intensities are reported in Table IV. The same procedure was followed for prediction of CH^{3+} states ionized in inner and valence shells. In this latter case, only states populated from the ground state of CH^+ were considered. It led to the consideration of four states (top states in Fig. 8) whose predicted intensities are given in Table V.

As in all molecules built with light atoms, the Auger decay rate largely dominates the x-ray fluorescence rate of core excited or core ionized molecules [16]. Relaxation of these four inner-shell ionized states by Auger effect will then occur. A proper calculation of the molecular Auger probability is not an easy task and has not been done here. We assumed that all transitions of the type $1\sigma^{-1} \rightarrow 2\sigma^{-2}$ and $1\sigma^{-1} \rightarrow 2\sigma^{-1}\, 3\sigma^{-1}$ were equally probable and predicted final populated states $^1\Sigma^+$ (pure $1\sigma^2\ 2\sigma$ configuration) and $^2\Sigma^+$ (pure $1\sigma^2\ 3\sigma$ configuration) on the basis of combinatorial considerations only. Triplet states of CH^{3+} were found to share equally between the two final states of CH^{4+}, whereas the $8\ ^1\Sigma^+$ state ($9\ ^1\Sigma^+$) was found to reach in 75% of cases the final $1\ ^2\Sigma^+$ ($2\ ^2\Sigma^+$) and in 25% of cases the $2\ ^2\Sigma^+$ ($1\ ^2\Sigma^+$). Another question concerns the competition between Auger relaxation and dissociation. The time at which Auger relaxation occurs will have a sizable effect on the KER value as illustrated in Fig. 10 for the case of pure Coulombic curves. Results of Fig. 10 were obtained by running a molecular dynamics code in which dissociation and Auger effect, of variable lifetime, were introduced. The same code was used for simulation of the "real case" depicted in Fig. 8. In that case we fitted, for sake of simplicity, the states of CH^{3+} and CH^{4+} with Coulombic curves of the form $\alpha + (\beta/R)$ with adjustable α and β parameters. It appeared that states of CH^{4+} are almost pure Coulombic curves since, fixing α to the theoretical value (dissociation limit), values of 2.82 and 2.99 were obtained for β, respectively, for $1\ ^2\Sigma^+$ and $2\ ^2\Sigma^+$, that is, close to the point charge value of 3. By contrast, the CH^{3+} curves could not be fitted well with α values equal to the dissociation limits so we let their values free in order to get a good fit of the curves in the 1.5 to 7 a.u. domain of internuclear distances.

C. Comparison between calculated and measured KER

Comparisons between predicted and measured KER are presented in Figs. 11 (CH^{2+} and CH^{3+}) and 12 (CH^{4+}). Measured KER were extracted from measured KER(H^+) values using formula (3), derived from momentum conservation law:

$$\mathrm{KER} = \mathrm{KER}(H^+)[\mathrm{M(CH)/M(C)}] = \mathrm{KER}(H^+)(13/12). \quad (3)$$

For calculated KER we report results obtained when considering the incident CH^+ in its ground state (black vertical lines) or in the metastable state (gray vertical lines). In order to be more visible, we reported intensities corresponding to the case where half of the CH^+ are in the ground state and half in the metastable state, although the contribution of metastable in the beam is likely to be lower. The arrows in Figs. 11 and 12 represent results of the PCCM model. Widths of the lines, due to the Franck-Condon region and experimental energy resolution (see before), are not shown. These widths, averaged over the different lines, are of the order of 4 eV (CH^{2+}), 7 eV (CH^{3+}), and 10 eV (CH^{4+}).

As seen in Fig. 11, KER values based on calculations of electronic excited states of CH^{2+} and CH^{3+} are in much better agreement with the experiment than PCCM predictions. We note that the difference between both calculations decreases with the charge, which is to be expected. In Fig. 12 we reported results of KER values in CH^{4+} on the basis of three assumptions concerning the Auger lifetime: very "short" lifetime [Fig. 12(a)], 20 fs lifetime [Fig. 12(b)], and very "long" lifetime [Fig. 12(c)]. Figure 12(a) corresponds to an immediate Auger effect as compared to dissociation which operates exclusively along the steep CH^{4+} curves. Figure 12(c) is opposite with dissociation entirely operating along the CH^{3+} curves. Both cases lead to a poor agreement with the experiment [especially Fig. 12(a)]. It is interesting to note that the difference between results derived from electronic excited states calculations and PCCM predictions is increasing with the Auger lifetime. Whereas close results are obtained in the absence of Auger effect [Fig. 12(a)], which is to be expected in CH^{4+}, a shift operates when the Auger effect is introduced which is due to the fact that the curves have different steepnesses as a function of R. Finally, the case where the Auger lifetime is equal to 20 fs [Fig. 12(b)] is the one leading to the best agreement with the experiment. This is very satisfactory since this is the lifetime we expect on the basis of what has been measured in C^+ (between 6 and 11 fs) [39] and C^{2+} ions (between 10 and 30 fs depending on the valence configuration) [40].

VII. INTERPRETATION OF KER(H^+) IN C_2H^{q+} AND C_3H^{q+} DISSOCIATIONS

For those two cases we restricted our analysis to a comparison between experiment and PCCM calculations. As seen in Figs. 5(b) and 5(c), deviations between experiment and PCCM predictions for KER(H^+) values are largely reduced as compared to the CH^{q+} case. It may be due to the fact that more states contribute and that there is a kind of average of all individual differences. Still a net discrepancy remains for C_2H^{q+}, $q \geqslant 5$ that is examined below.

For C_2H^{q+} $q \geqslant 5$, single inner-shell ionization and double inner-shell ionization for the highest charges are contributing in a dominant way to the ion production (see Table I). We then introduced, in a similar way as before, single and double Auger relaxation in the three-body code of classical molecular dynamics. The Auger lifetime Γ_A was varied, and taken the same in the case of relaxation by one or two Auger processes. We present in Table VI the KER(H^+) values calculated for various Auger lifetimes Γ_A for the channels of interest and for single (S) as well as double (D) Auger relaxation. Double Auger relaxation, which induces an increase of +2 of the molecule charge, leads to a much larger correction of KER(H^+) than single Auger. The case $\Gamma_A \sim 20$ fs is of particular interest, as it was shown to reproduce well the experiment on CH^{4+} (see Fig. 12) and it is also a plausible value on the basis of what is known in C^{q+} ions. We present in Fig. 13 KER(H^+) values calculated with $\Gamma_A = 20$ fs and resulting from a weighting of KER(H^+) due to inner-shell ionization (single and double) and due to pure valence ionization, following percentages given in Table I. Results are reported in Fig. 13, as a broken line. As

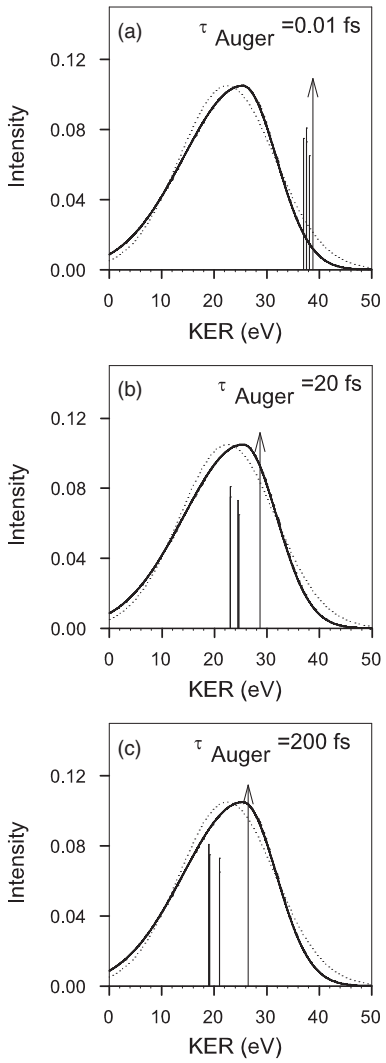

FIG. 12. Comparison between measured KER distributions (solid and dotted curves, see Sec. II) and calculated KER (vertical black lines) in C^{3+}-H^+ dissociation as a function of the inner-shell vacancy Auger lifetime. Arrows correspond to PCCM predictions.

seen in Fig. 13, corrected PCCM predictions are now inside the experimental error bars.

For C_3H^{q+} [see Fig. 5(c)], the comparison between experiment and PCCM predictions is satisfactory for all considered q values. We nevertheless performed the corrections due to

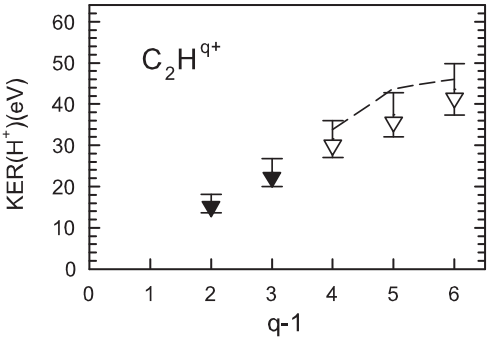

FIG. 13. Comparison between measured KER(H^+) and PCCM predictions corrected from Auger with a lifetime of 20 fs (dashed line) for the dissociation of C_2H^{q+}, $q = 5$–7.

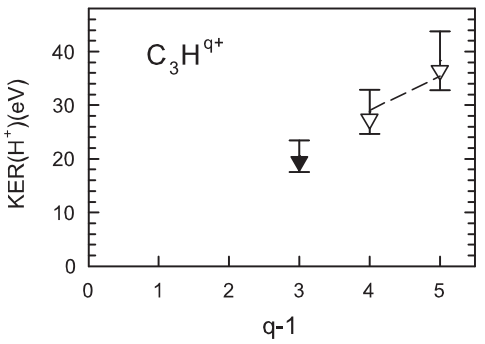

FIG. 14. Same legend as Fig. 13 for dissociation of C_3H^{q+}, $q = 5$–6.

inner-shell ionization followed by Auger relaxation, as in previous cases, working with a four-body code of classical molecular dynamics. In Table VII KER(H^+) values calculated for various Auger lifetimes Γ_A for the channels of interest are reported and in Fig. 14 corrected KER(H^+), performed with $\Gamma_A = 20$ fs, and weighted according to percentages of Table I are reported as a broken line. As seen in Fig. 14, the corrected-Auger PCCM KER(H^+) values agree with the measured ones.

VIII. CONCLUSIONS

In conclusion we have performed measurements of ionization cross sections and dissociation branching ratios of multiply charged species produced in $v_p = 4.5$ a.u. C_nH^+ ($n \leqslant 4$)-He collisions, as well as measurements of partial branching ratios for channels involving H^+ emission and associated KER(H^+) of multiply charged species produced in $v_p = 3.6$ a.u. C_nH^+ ($n \leqslant 3$)-He collisions. The first set of data was useful to check the validity of the IAE model for ionization cross sections calculations, the contribution of inner-shell ionization and also useful for checking the partial branching ratios measured in the second type of experiment. For channels involving H^+ emission selected in this second type of experiment, we measured KER(H^+) values considerably lower than predictions of the point charge Coulomb model (PCCM) for CH^{q+} ($q \leqslant 4$) dissociation and, in a less extent, for C_2H^{q+} dissociation. *Ab initio* calculations of electronic excited states of CH^{q+} performed within the MRCI approach as well as predictions of their population intensities allowed a perfect understanding of measured KER distributions. Another result was the extraction of an Auger lifetime for an inner-shell vacancy in CH^{3+} whose value (∼20 fs) is close to Auger lifetimes measured in C^{q+} atomic ions. This Auger lifetime, introduced in the PCCM model, allowed also to satisfactorily reproduce measured KER(H^+) in the case of dissociation of C_2H^{q+} and C_3H^{q+} molecular ions. The PCCM approach, when corrected, appeared then to be reasonably good for predictions of KER(H^+) in dissociation of C_2H^{q+} ($q \geqslant 5$) and C_3H^{q+} ($q \geqslant 4$).

ACKNOWLEDGMENTS

The authors are indebted to Michel Barat, Jacqueline Fayeton, and Bruno Lucas for their help in the preparation and during the experiment. They thank Jacky Liévin for fruitful discussions.

APPENDIX

Branching ratios for incident C_nH^+ projectiles at 4.5 a.u. (see Sec. IV A) are given in Table VIII below

TABLE VIII. Measured dissociation branching ratios of C_nH^{q+} molecules produced in 4.5 a.u. C_nH^+-He collisions.

CH^{q+} Channel	q	BR (%) (abs. error)	C_2H^{q+} Channel	q	BR (%) (abs. error)
$C^+\|H^+$	2	83.5 (1.4)	$C^+\|CH^+$	2	41.6 (5.1)
$C^{2+}\|H$		16.5 (0.3)	$C_2{}^+\|H^+$		23.0 (2.1)
			$C^+\|C\|H^+$		22.5 (2.6)
			$2C^+\|H$		12.1 (1.0)
			$2C^+\|H^+$	3	87.4 (5.2)
			$C^{2+}\|C\|H^+$		7.6 (1.0)
			$C^{2+}\|C^+\|H$		4.8 (0.4)
			$C^{2+}\|C^+\|H^+$	4	97.9 (2.3)
			$2C^{2+}\|H$		2.1 (0.5)
C_3H^{q+} Channel	q	BR (%) (abs. error)	C_3H^{q+} Channel	q	BR (%) (abs. error)
$C_2H^+\|C^+$	2	29.8 (3.0)	$H\|3C^+$		5.5 (0.7)
$C_3{}^+\|H^+$		19.9 (1.5)	$2C\|C^{2+}\|H^+$		0.9 (0.4)
$C_2{}^+\|CH^+$		12.3 (0.7)	$C^+\|CH^+\|C^{2+}$	4	12.6 (2.7)
$C\|C^+\|CH^+$		8.1 (0.7)	$C_2{}^+\|C^{2+}\|H^+$		0.9 (0.7)
$H\|C_2{}^+\|C^+$		6.7 (0.5)	$3C^+\|H^+$		65.5 (6.0)
$C\|C_2{}^+\|H^+$		3.9 (0.5)	$C\|C^+\|C^{2+}\|H^+$		17.2 (3.0)
$C_2\|C^+\|H^+$		3.2 (0.5)	$H\|2C^+\|C^{2+}$		3.2 (0.5)
$CH\|2C^+$		1.8 (0.75)	$2C^+\|C^{2+}\|H^+$	5	91.3 (10.0)
$C\|H\|2C^+$		7.3 (0.75)	$C\|2C^{2+}\|H^+$		4.1 (3.0)
$2C\|C^+\|H^+$		6.5 (0.6)	$H\|C^+\|2C^{2+}$		2.1 (1.0)
$C_3{}^{++}\|H^+$	3	1.7 (0.5)	$C\|C^+\|C^{3+}\|H^+$		1.9 (1.4)
$C_2{}^+\|C^+\|H^+$		21.5 (2.7)	$C^+\|2C^{2+}\|H^+$	6	84.3 (27)
$2C^+\|CH^+$		20.1 (2.7)	$2C^+\|C^{3+}\|H^+$		10.6 (6.6)
$CH\|C^+\|C^{2+}$		3.6 (1.5)	$C\|C^{2+}\|C^{3+}\|H^+$		4.2 (2.8)
$C\|CH^+\|C^{2+}$		3.3 (1.0)	$3C^{2+}\|H^+$	7	50.3 (34.2)
$C_2\|C^{2+}\|H^+$		0.10 (0.1)	$C^+\|C^{2+}\|C^{3+}\|H^+$		49.7 (38)
$C\|2C^+\|H^+$		41.7 (2.5)			
C_4H^{q+} Channel	q	BR (%) (abs. error)	C_4H^{q+} Channel	q	BR (%) (abs. error)
C_4H^{2+}	2	3.3 (0.2)	$H\|C_2{}^+\|2C^+$	3	5. 2 (0.2)
$C_3H^+\|C^+$		39.7 (2.5)	$2C\|2C^+\|H^+$		23.3 (0.4)
$C_3{}^+\|CH^+$		4.5 (0.8)	$C\|H\|3C^+$		7.1 (0.4)
$C_2{}^+\|C_2H^+$		3.6 (0.5)	$C_2{}^+\|2C^+\|H^+$	4	24.6 (1.5)
$C_4{}^+\|H^+$		3.1 (0.2)	$3C^+\|CH^+$		4.8 (4.4)
$H\|C_3{}^+\|C^+$		10 .0 (0.2)	$C\|3C^+\|H^+$		55.9 (1.5)
$C\|C_3{}^+\|H^+$		2.9 (0.1)	$2C\|C^+\|C^{2+}\|H^+$		4.6 (0.5)
$C_2\|C^+\|CH^+$		2.3 (0.3)	$H\|4C^+$		3.4 (0.3)
$C\|C_2H^+\|C^+$		2.1 (0.6)	$C\|H\|2C^+\|C^{++}$		2.0 (0.5)
$C\|C_2{}^+\|CH^+$		2.1 (0.3)	$C_2{}^+\|C^+\|C^{2+}\|H^+$	5	3.8 (1.0)
$H\|2C_2{}^+$		2.0 (0.1)	$2C^+\|CH^+\|C^{2+}$		1.6 (4.0)
$C_3\|C^+\|H^+$		1.7 (0.1)	$4C^+\|H^+$		60.4 (3.4)
$C_2\|C_2{}^+\|H^+$		1.2 (0.1)	$C\|2C^+\|C^{2+}\|H^+$		29.2 (2.6)
$CH\|C_2{}^+\|C^+$		1.0 (0.3)	$3C^+\|C^{2+}\|H^+$	6	79 (9)
$C\|H\|C_2{}^+\|C^+$		4.3 (0.2)	$C\|2C^+\|C^{3+}\|H^+$		2.2 (1.2)
$C_2\|C\|C^+\|H^+$		2.7 (0.1)	$C\|C^+\|2C^{2+}\|H^+$		16.6 (3.6)
$C_2\|H\|2C^+$		2.2 (0.1)	$H\|2C^+\|2C^{2+}$		2.0 (0.5)
$2C\|C_2{}^+\|H^+$		2.1 (0.1)	$2C^+\|2C^{2+}\|H^+$	7	81 (19)
$2C\|C^+\|CH^+$		1.8 (0.6)	$3C^+\|C^{3+}\|H^+$		8 (5)
$2C\|H\|2C^+$		3.1 (0.2)	$C\|3C^{2+}\|H^+$		7 (4)
$3C\|C^+\|H^+$		2.5 (0.1)	$C\|C^+\|C^{2+}\|C^{3+}\|H^+$		4 (3)
$C_3H^{2+}\|C^+$	3	3.1 (0.1)	$C^+\|3C^{2+}\|H^+$	8	64 (47)
$C_3{}^+\|C^+\|H^+$		12.8 (0.5)	$2C^+\|C^{2+}\|C^{3+}\|H^+$		25 (25)
$C_2{}^+\|C^+\|CH^+$		5.8 (1.1)	$C\|2C^{2+}\|C^{3+}\|H^+$		8.5 (8.5)
$2C_2{}^+\|H^+$		5.5 (0.3)	$H\|C^+\|2C^{2+}\|C^{3+}$		1.7 (1.7)
$C_2H^+\|2C^+$		4.2 (1.1)	$C^+\|2C^{2+}\|C^{3+}\|H^+$	9	66 (45)
$C\|2C^+\|CH^+$		3.8 (1.0)	$4C^{2+}\|H^+$		24 (17)
$C\|C_2{}^+\|C^+\|H^+$		19.9 (0.6)	$2C^+\|2C^{3+}\|H^+$		7 (7)
$C_2\|2C^+\|H^+$		5.9 (0.3)	$C\|C^{2+}\|2C^{3+}\|H^+$		2 (2)

[1] D. Mathur, Phys. Rep. **391**,1 (2004).
[2] M. Chabot, F. Mezdari, K. Béroff, G. Martinet, and P. A. Hervieux, Phys. Rev. Lett. **104**, 043401 (2010).
[3] I. Plesser, Z. Vager, and R. Naaman, Phys. Rev. Lett. **56**, 1559 (1986).
[4] E. Baldit, S. Saugout, and C. Cornaggia, Phys. Rev. A **71**, 021403 (2005).
[5] J. Gagnon, K. F. Lee, D. M. Rayner, P. B. Corkum, and V. R. Bhardwaj, J. Phys. B **41,** 215104 (2008).
[6] C. Cornaggia, Laser Phys. **19,** 1660 (2009).
[7] A. Matsuda, M. Fushitani, E. J. Takahashi, and A. Hishikawa, Phys. Chem. Chem. Phys **13**, 8697 (2011).
[8] U. Werner, B. Sieg Tmann, R. Mann, N. M. Kabachnik, and H. O. Lutz, Phys. Scripta T **92**, 244 (2001).
[9] U. Werner, K. Beckord, J. Becker, H. O. Folkerts, and H. O. Lutz Nucl. Instrum. Methods B **98,** 385 (1995).
[10] F. A. Rajgara, M. Krishnamurthy, D. Mathur, T. Nishide, T. Kitamura, H. Shiromaru, Y. Achiba, and N. Kobayashi, Phys. Rev. A **64,** 032712 (2001).
[11] M. Tarisien *et al*., J. Phys. B **33,** L11 (2000).
[12] J. Rajput and C. P. Safvan Phys. Rev. A **75,** 062709 (2007).
[13] J. S. Wright, G. A. DiLabio, D. R. Matusek, P. B. Corkum, M. Y. Ivanov, C. Ellert, R. J. Buenker, A. B. Alekseyev, and G. Hirsch, Phys. Rev. A **59**, 4512 (1999).
[14] S. De, J. Rajput, A. Roy, P. N. Ghosh, and C. P. Safvan, Phys. Rev. A **77,** 022708 (2008).
[15] F. A. Rajgara *et al*., J. Phys. B **37,** 1699 (2004).
[16] I. Nenner and P. Morin, *VUV and Soft X-ray Photoioization*, edited by U. Becker and D. A. Shirley (Plenum, New York, 1996), p. 291.
[17] C. A. Tachino, M. E. Galassi, and R. D. Rivarola, Phys. Rev. A **80**, 014701 (2009).
[18] A. E. Bannister, H. F. Krause, C. R. Vane, N. Djuric, D. B. Popovic, M. Stepanovic, G. H. Dunn, Y. S. Chung, A. C. H. Smith, and B. Wallbank, Phys. Rev. A **68,** 042714 (2003).
[19] J. P. Gu, G. Hirsch, R. J. Buenker, M. Kimura, C. M. Dutta, and P. Nordlander, Phys. Rev. A **57,** 4483 (1998).
[20] S. E. Butler, S. L. Guberman, and A. Dalgarno, Phys. Rev. A **16,** 500 (1977).
[21] M. Chabot *et al*., Nucl. Instrum. Methods B **197,** 155 (2002).
[22] T. Tuna *et al*., J. Chem. Phys. **128,** 124312 (2008).
[23] K. Wohrer, M. Chabot, R. Fossé, and D. Gardes, Rev. Sci. Instrum. **71,** 2025 (2000).
[24] M. Lampton and C. W. Carlson, Rev. Sci. Instrum. **50,** 1093 (1979).
[25] K. Wohrer and R. L. Watson, Phys. Rev. A **48,** 4784 (1993).
[26] Z. Amitay, D. Zajfman, P. Forck, U. Hechtfischer, B. Seidel, M. Grieser, D. Habs, R. Repnow, D. Schwalm, and A. Wolf, Phys. Rev. A **54,** 4032 (1996).
[27] K. Hashimoto, S. Iwata, and Y. Osamura, Chem.Phys. Lett. **174,** 649 (1990).
[28] J. Yang, J. Y. Qi, M. D. Chen, Q. E. Zhang, and C. T. Au, Int. J. Mass. Spectrom. Ion Phys. **272,** 165 (2008).
[29] U. Werner, N. M. Kabachnik, V. N. Kondratyev, and H. O. Lutz, Phys. Rev. Lett. **79,** 1662 (1997).
[30] T. Tuna, University Paris Sud 11, 2008.
[31] MOLPRO, version 2010.1, a package of ab initio programs, H.-J. Werner *et al*., see [http://www.molpro.net].
[32] C. E. Moore, Atomic Energy Levels NSRDS-NBS 35/Vol I (1971).
[33] H. Nakatsuji and S. Saito Int. J. Quantum. Chem. **39,** 93 (1991).
[34] R. L. Martin and D. A. J. Shirley, Chem. Phys **64,** 3685 (1976); Phys. Rev. A **13,** 1475 (1976).
[35] P. W. Langhoff, S. R. Langhoff, T. N. Rescigno, J. Schirmer, L. S. Cederbaum, W. Domcke, and W. Vonniessen, Chem. Phys. **58,** 71 (1981).
[36] S. Krummacher, V. Schmidt, F. Wuilleumier, J. M. Bizau, and D. Ederer, J. Phys. B **16,** 1733 (1983).
[37] L. S. Cederbaum and W. Domcke, Adv. Chem. Phys. **36**, 205 (1977); L. S. Cederbaum, W. Domcke, J. Schirmer, and W. von Niessen, *ibid*. **65**, 115 (1986).
[38] F. Tarantelli, Chem..Phys **329**, 11 (2006).
[39] A. S. Schlachter *et al*., J. Phys. B **37,** L103 (2004).
[40] S. W. J. Scully *et al*., J. Phys. B **38,** 1967 (2005).